AGU PUBLICATIONS

Geophysical Research Letters

RESEARCH LETTER
10.1002/2017GL072605

Key Points:
- Observation of a new population of suprathermal (1.5–3 times the solar wind energy) H^+ around the Moon
- Source located above the lunar surface (>500 km) in the sunward direction
- Possible source mechanisms are considered, but an additional mechanism is required to fully explain the new population

Supporting Information:
- Supporting Information S1

Correspondence to:
M. B. Dhanya and A. Bhardwaj,
mb_dhanya@vssc.gov.in;
ABhardwaj@prl.res.in

Citation:
Dhanya, M. B., A. Bhardwaj, Y. Futaana, S. Barabash, M. Wieser, M. Holmström, and P. Wurz (2017), New suprathermal proton population around the Moon: Observation by SARA on Chandrayaan-1, *Geophys. Res. Lett.*, *44*, 4540–4548, doi:10.1002/2017GL072605.

Received 12 JAN 2017
Accepted 4 MAY 2017
Accepted article online 9 MAY 2017
Published online 27 MAY 2017

New suprathermal proton population around the Moon: Observation by SARA on Chandrayaan-1

M. B. Dhanya[1], Anil Bhardwaj[1,2], Yoshifumi Futaana[3], Stas Barabash[3], Martin Wieser[3], Mats Holmström[3], and Peter Wurz[4]

[1]Space Physics Laboratory, Vikram Sarabhai Space Center, Trivandrum, India, [2]Physical Research Laboratory, Ahmedabad, India, [3]Swedish Institute of Space Physics, Kiruna, Sweden, [4]Physikalisches Institut, University of Bern, Bern, Switzerland

Abstract We report a new population of suprathermal H^+ (~1.5–3 times the solar wind energy) around the Moon observed by Solar Wind Monitor (SWIM)/Sub-keV Atom Reflecting Analyzer (SARA) on Chandrayaan-1. These ions have large initial velocity (>100 km s^{-1}) and are observed on the dayside, near the terminator, and in the near-wake region (100–200 km above the surface), when the Moon is located outside Earth's bow shock. Backtracing suggests that the source is located >500 km above the dayside lunar surface. Possible sources considered for these ions are ionization of backscattered lunar energetic neutral hydrogen atoms, ionization of lunar exospheric hydrogen, inner source pickup ions, interstellar pickup ions, ionization of neutral solar wind, and solar wind H^+ reflected from Earth's bow shock. The comparison of the observed flux (density) with that expected from these sources and the velocity distribution suggests that an additional source is required to explain the population.

1. Introduction

The Moon is a regolith-covered planetary object characterized by a surface boundary exosphere [*Stern*, 1999; *Cook et al.*, 2013; *Wurz et al.*, 2007] and with localized magnetic anomalies on the surface [*Richmond and Hood*, 2008; *Tsunakawa et al.*, 2015, and references therein]. Solar wind plasma interacts continuously with the lunar surface thereby controlling the lunar plasma environment [*Halekas et al.*, 2011; *Bhardwaj et al.*, 2015]. Observations from different missions have shown the presence of several populations of energetic ions around the Moon, such as solar wind protons scattered from the dayside lunar surface [*Saito et al.*, 2008; *Holmström et al.*, 2010] and magnetic anomalies [*Lue et al.*, 2011; *Saito et al.*, 2010], and lunar exospheric ions picked up by the solar wind [*Hilchenbach et al.*, 1992; *Mall et al.*, 1998; *Wang et al.*, 2011; *Halekas et al.*, 2013, 2015, 2016; *Poppe et al.*, 2016].

There are a few mechanisms by which solar wind protons enter the near-wake region (100–200 km above the nightside surface). Direct entry of solar wind to the lunar wake includes diffusion of solar wind protons parallel to the interplanetary magnetic field (B_{IMF}) [*Futaana et al.*, 2010], due to larger gyroradii [*Dhanya et al.*, 2013] and due to an increase in gyroradii aided by the wake boundary electric field [*Nishino et al.*, 2009a]. In addition, solar wind scattered from the lunar surface can enter the near-wake region along trajectories consistent with B_{IMF} and the convective electric field (E_c) of the solar wind [*Nishino et al.*, 2009b; *Wang et al.*, 2010]. Using observations by the Solar Wind Monitor (SWIM) of the Sub-keV Atom Reflecting Analyzer (SARA) experiment on Chandrayaan-1, *Dhanya et al.* [2016] have shown that there are a few ion populations in the near wake whose source mechanism(s) is(are) yet to be identified, which include populations with energies higher than that of solar wind.

Here we present the analysis of suprathermal protons (~1.5–3 times the solar wind energy) observed on the dayside, near the terminator, and in the near-lunar wake region, by SWIM/SARA on Chandrayaan-1. These observations provide insight into possible processes which may contribute to the lunar plasma environment.

2. Instrumentation and Data Sources

SWIM was an ion mass analyzer of the SARA experiment on Chandrayaan-1, which operated at altitudes of 100 and 200 km [*Bhardwaj et al.*, 2005; *Barabash et al.*, 2009]. SWIM worked in the energy range 100–3000 eV/q ($\Delta E/E$ ~7%) and had a fan-shaped field of view (FOV) subdivided into 16 angular pixels. The pixel size is 7.6°

full width at half maximum in elevation direction and varies from 6.4° to 17.6° full width at half maximum in azimuthal direction, depending on viewing direction. Assisted by the nadir-pointing spacecraft motion, the FOV covers $\sim 2\pi$ within half of the orbit (more details about SWIM are provided in *Futaana et al.* [2010], *Bhardwaj et al.* [2012], and *Dhanya et al.* [2013, 2016]).

Advanced Composition Explorer (ACE) level 2 data from the Solar Wind Electron, Proton, and Alpha Monitor (SWEPAM) and magnetometer (MAG) instruments are used to obtain the solar wind parameters, after time shift to the location of the Moon [*Dhanya et al.*, 2016]. Data from the Wind satellite is used during gaps in the ACE data.

The observations reported here are for a time period when the Moon was outside the Earth's bow shock. For the analysis, we have used an aberrated lunar-centered solar ecliptic coordinate system (aLSE), where the *x* axis is antiparallel to the solar wind velocity (v_{sw}), the *z* axis is toward ecliptic north, and the *y* axis completes the right-handed coordinate system (illustrated in Figure 1 of *Dhanya et al.* [2016]). In addition, the observations are transformed into the solar wind rest frame to discuss the velocity distribution of the ions in 2-D velocity space (parallel and perpendicular to B_{IMF}).

A backtracing model (details in *Dhanya et al.* [2016]) has been used to construct the particle trajectories under Lorentz force in aLSE coordinates. The magnetic field used in the model is essentially B_{IMF}, which is enhanced by a factor of 1.5 inside the wake (B_{wake}) [*Colburn et al.*, 1967]. The electric field consists of E_c, and the wake boundary electric field (E_{wake}) of magnitude 0.7 mV m^{-1} [*Halekas et al.*, 2005; *Nishino et al.*, 2009a]. The computation proceeds until the particle trajectory either hits the lunar surface or has traveled a sufficiently large distance (>5000 km) upstream. Based on the backtracing, we arrived at an event selection criterion, which is presented in the supporting information (Figure S1). The observations discussed in this paper have a signal strength well above the background.

3. Observation

The energy-time spectrogram from the SWIM observations in orbit 1915 on 15 April 2009 (13:29 to 15:27 UT) along with the prevailing solar wind conditions (from ACE time shifted to the location of the Moon) are shown in Figure 1. During this orbit, Chandrayaan-1 was at 100 km altitude with an orbital period of ~120 min. SWIM made measurements on both dayside and nightside of the Moon. The strong signal seen around 15.0 h UT (marked as "A") corresponds to solar wind observations on the dayside. The signal "B" with energies comparable to that of solar wind corresponds to the protons in the near-wake region. The population marked as "C" observed across the terminator to the nightside of the Moon, with energies as high as 2.5–3 times that of solar wind (>1800 eV) is of interest and is analyzed further. From Figures 1b–1e, it can be seen that during this period, the solar wind speed was on an average ~300 km s^{-1}, B_{IMF} ~5 nT, with azimuth angle ~ 230° and zenith angle 50°–70°, and E_c ~1.5 mV m^{-1}. The position of the Moon relative to the Earth, illustration of SWIM FOV, and the orbit of Chandrayaan-1 around the Moon are shown in Figures 1f–1h, respectively.

To understand the origin of the high-energy ions, it is important to know the mass (m/q) and initial velocity of the ions. SWIM has a mass resolution $m/\Delta m \sim 1.5$ [*Wieser and Barabash*, 2016]. This is sufficient to separate $m/q = 1$ from $m/q = 2$ provided only one of the two masses is present. For the present analysis the signals are consistent with $m/q = 1$, with an estimated maximum $m/q = 2$ contribution of less than 10%. Hence, in our analysis we use $m/q = 1$.

The velocity distribution of the ions is analyzed to infer their initial velocity. Ions moving under electric and magnetic fields (E_c and B_{IMF} in this context) form a ring-shaped velocity distribution in the plane defined by the velocity component parallel to E_c (v_E), and the velocity component perpendicular to both E_c and B_{IMF} (v_C). In other words, v_C is the ion velocity component parallel to $v_{sw_\perp}$, where $v_{sw_\perp}$ is the component of v_{sw} perpendicular to B_{IMF}. For ions with zero initial velocity, the ring-shaped distribution is expected to be centered around ($v_{sw_\perp}$,0), with a radius of $v_{sw_\perp}$ [*Futaana et al.*, 2003]. For ions of $m/q = 1$ and nonzero initial velocity, the radius of the distribution can be greater or smaller than $v_{sw_\perp}$ depending on whether the direction of the initial velocity is antiparallel or parallel to the solar wind velocity, respectively. The velocity distribution of the population "C" in the v_C-v_E plane, normalized to $v_{sw_\perp}$ is shown in Figure 2a. Also, Figure 2a shows the expected velocity distribution for ions of $m/q = 1$ with zero initial velocity (dashed circle), for reference. The data points lie well outside this circle, and form a ring distribution with center (+1, 0) and radius between 1.5

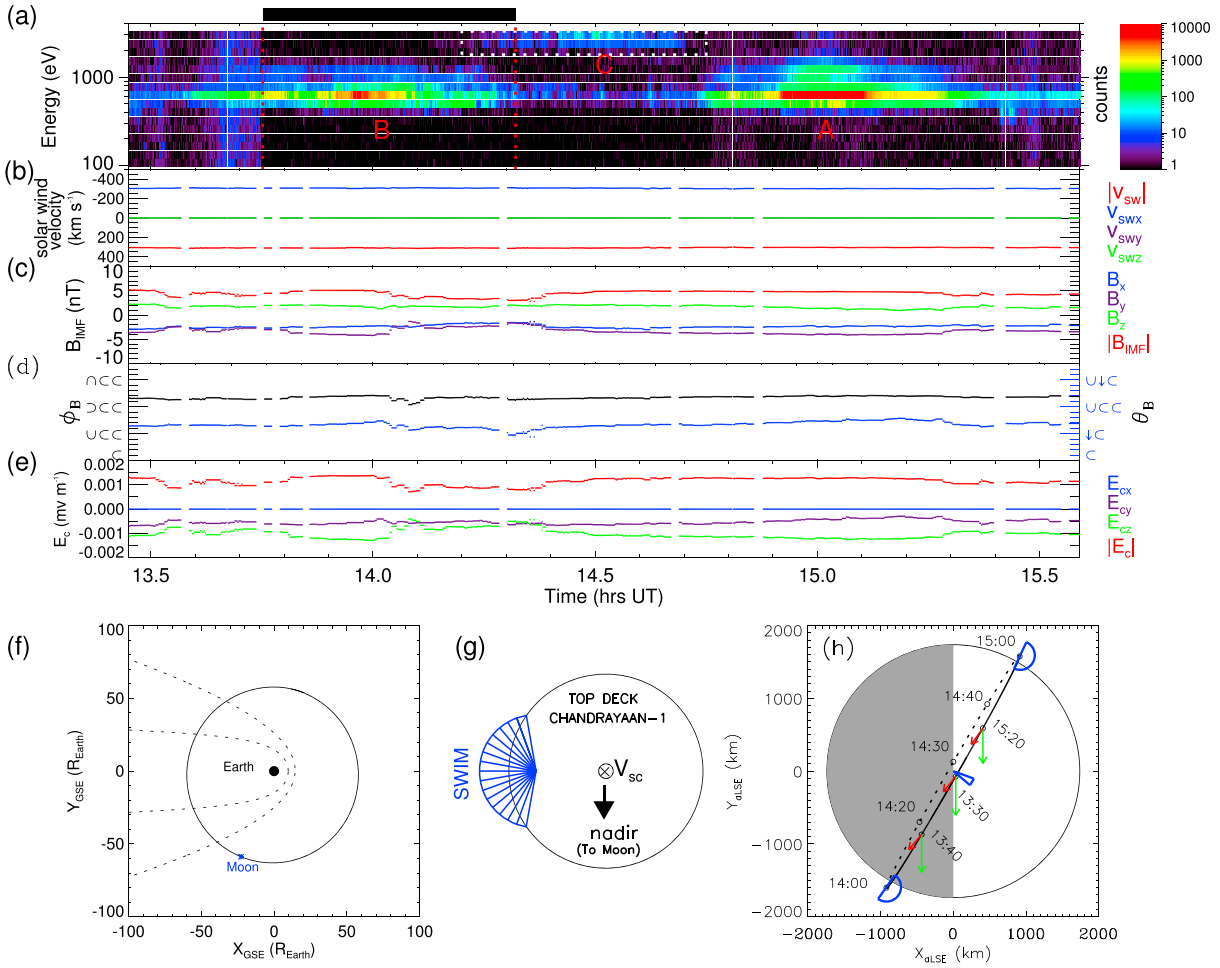

Figure 1. (a) Energy-time spectrogram from SWIM observations in orbit 1915 on 15 April 2009 during ~13:30–15:30 UT. The black filled box on the top of the panel indicates the time interval when SWIM made observations in the lunar wake. The red dotted vertical lines mark wake entry and exit timings. The high-energy signals (>1800 eV) across the terminator to the wake are enclosed within the white rectangle. (b) Magnitude of the solar wind velocity ($|v_{sw}|$) and the components ($v_{swx}, v_{swy}, v_{swz}$). (c) Magnitude of the interplanetary magnetic field: $|B_{IMF}|$ (red) and components B_x (blue), B_y (violet), and B_z (green). (d) Orientation of B_{IMF} in terms of azimuth angle (ϕ_B) and zenith angle (θ_B). (e) Magnitude, $|E_c|$ (red), of the convective electric field of the solar wind, and the components E_{cx} (blue), E_{cy} (violet), and E_{cz} (green). (f) Lunar orbit around the Earth in April 2009 in Geocentric Solar Ecliptic (GSE) coordinates; GSE has its origin on the Earth center; the x axis is toward the Sun, z axis toward ecliptic north, and y axis completes the right-handed coordinate system. The position of the Moon on 15 April 2009 is indicated by an asterisk (blue). (g) Schematic of the SWIM FOV (blue), which is divided into 16 angular pixels. SWIM was mounted on the top deck of Chandrayaan-1. The direction of nadir and the velocity vector of the spacecraft (V_{sc}) are shown. V_{sc} is antiparallel to the direction of normal to the mounting plane of SWIM during this orbit. (h) Orbit of Chandrayaan-1 around the Moon during orbit 1915 projected in the x-y plane of aLSE coordinates as viewed from z_{aLSE}. The black solid curve indicates the part of orbit with $z_{aLSE} > 0$, and black dotted curve is with $z_{aLSE} < 0$. The positions of Chandrayaan-1 at four time instants are also indicated. Schematic of FOV (blue) of SWIM is shown overlaid on the orbit close to the pole, dayside, and nightside equator. The geometry of B_{IMF} (red arrow) and E_c (green arrow) in the x-y plane are also shown for a few time instants. The solar wind parameters in Figures 1b–1e are in aLSE coordinates.

(inner dotted circle) and 1.9 (outer dotted circle), indicating that the ions with $m/q = 1$ are of nonthermal origin with an initial velocity antiparallel to the solar wind.

The component of the ion velocity parallel to B_{IMF} (v_B) is considered as a component of the initial velocity, since v_B is conserved for motion under mutually perpendicular electric and magnetic fields (B_{IMF} and E_c). The velocity distribution of ions in the v_B-v_E plane (Figure 2b) shows v_B to be as large as 200 km s^{-1}, suggesting the ions to be nonthermal. The pitch angle distribution of the ions (Figure 2c) indicates that the ions have their dominant velocity component perpendicular to B_{IMF}.

The velocity distribution of the ions of population "C" in the solar wind rest frame, where the velocities are resolved into components parallel to B_{IMF} ($v_{||}$) and perpendicular to B_{IMF} ($v_{\perp}$) (similar to the method discussed in *Dhanya et al.* [2016]) is shown Figure 2d. For reference, the velocity distribution of the actual solar wind at the location of the Moon (time-shifted ACE data) is also shown in Figure 2d (asterisk symbol) in

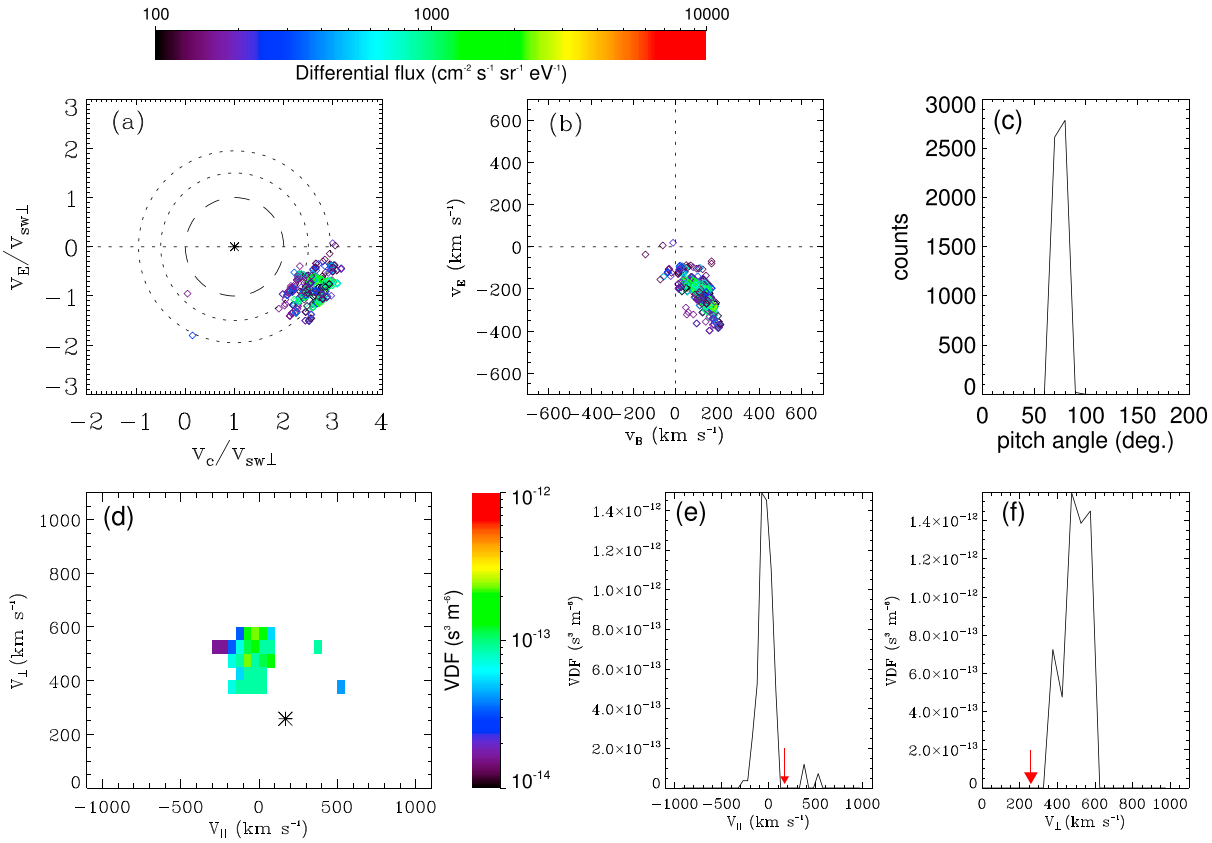

Figure 2. (a) Normalized velocity distribution in the v_c-v_E plane for the high-energy event ("C") in orbit 1915. v_c is the ion velocity component perpendicular to both E_c and B_{IMF}, and v_E is the ion velocity parallel to E_c. The value of $v_{sw\perp}$ is the value averaged over the time interval of the high-energy event (~260 km s^{-1}). The dashed inner circle is centered at (+1, 0) indicated by an asterisk with unit radius and represents the distribution expected for zero initial velocity ions of $m/q = 1$. The two dashed inner and outer circles centered at (1,0), and passing through the data points with radius = 1.5 and 1.9, respectively, represent the boundaries of the ring-shaped distribution. (b) Velocity distribution in the v_B-v_E plane, where v_B is the component of ion velocity parallel to B_{IMF}. (c) Pitch angle distribution of the ions. (d) Velocity distribution in the solar wind rest frame. The horizontal axis refers to the component of the ion velocity parallel to B_{IMF} ($v_{||}$), and the vertical axis refers to the component of the ion velocity perpendicular to B_{IMF} ($v_\perp$). The velocity components of the upstream solar wind averaged over the time interval of interest in the aLSE coordinates are indicated by the asterisk symbol. (e) One-dimensional cut through the velocity distribution along $v_{||}$ in the solar wind rest frame. The red arrow indicates the value of $v_{sw_{||}}$ ~165 km s^{-1} in aLSE coordinates. (f) One-dimensional cut through the velocity distribution along $v_\perp$ in the solar wind rest frame. The red arrow indicates the value of $v_{sw_\perp}$ ~260 km s^{-1} in aLSE coordinates.

aLSE coordinates. The 1-D line plots of this 2-D distribution along the x and y axes are shown in Figures 2e and 2f, respectively. Figure 2e is generated by summing the distribution over $v_\perp$ bins and Figure 2f by summing the distribution over $v_{||}$ bins. Figures 2d–2f show that in the solar wind rest frame the ion velocity component perpendicular to the B_{IMF} is as high as $> 2\times v_{sw_\perp}$, confirming that the ions must have had a substantial velocity component antiparallel to the solar wind at their origin.

3.1. Trajectory Calculations

To investigate the source of these suprathermal ions further, the trajectories of the ions are constructed using a backtracing model [*Dhanya et al.*, 2016]. Backtracing shows that most (>99%) of these nonthermal ions originate on the subsolar side of the Moon with a negligible contribution (≪1%) from the lunar surface. The trajectories in Figures 3a–3f show that the observed ions pass through the minimum height of the cycloid at altitudes >500 km above the dayside lunar surface, indicating a high-altitude source. This is further seen from the plot of the speed of these ions as a function of the altitude above the dayside lunar surface (Figure 3g). The altitude range where the velocity becomes minimal shows an extended source located at altitude >500 km. Also, Figure 3g shows that the minimum speed of the ions at any altitude is ≳200 km s^{-1} (antiparallel to the solar wind). Hereafter, the suprathermal H^+ population "C" in the orbit 1915 is referred to as Event 1.

As seen from Figure 1a, the signal strength of Event 1 observed during 14.2–14.75 h UT (~35 min) is ~10–100 counts. The ions are observed mostly in three angular pixels of SWIM. Integrating the differential

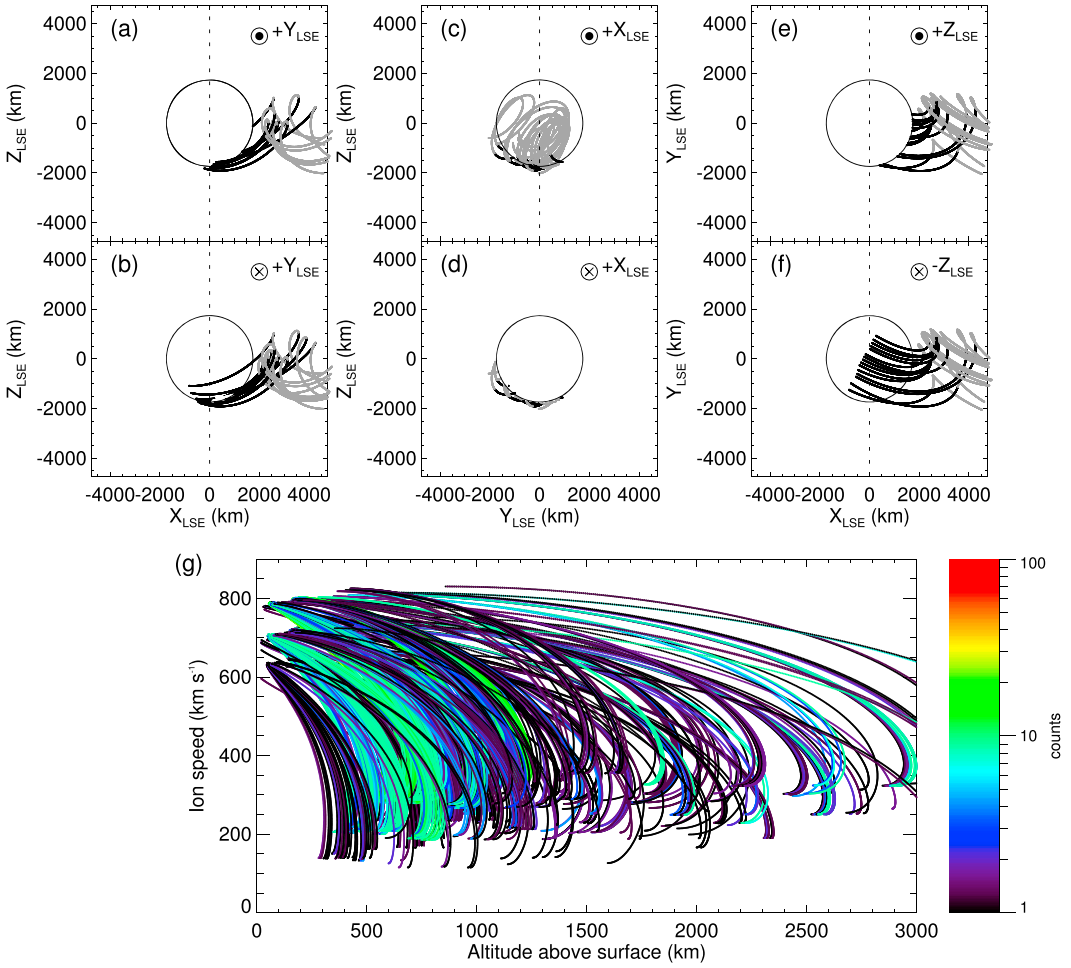

Figure 3. Trajectories of ions which terminate high above the dayside lunar surface during the backtracing projected in different planes in aLSE coordinates. (a) x_{aLSE}-z_{aLSE} plane as viewed from $+y_{aLSE}$, (b) x_{aLSE}-z_{aLSE} plane as viewed from $-y_{aLSE}$, (c) y_{aLSE} -z_{aLSE} plane as viewed from $+x_{aLSE}$, (d) y_{aLSE}-z_{aLSE} plane as viewed from $-x_{aLSE}$, (e) x_{aLSE}-y_{aLSE} plane as viewed from $+z_{aLSE}$, and (f) x_{aLSE}-y_{aLSE} plane as viewed from $-z_{aLSE}$. In each panel, the black curves indicate the first part of the trajectories (before the first velocity minimum) as backtraced from the observed location. The remaining part of the trajectory is shown in grey. (g) Ion speed during backtracing as a function of altitude above the dayside lunar surface. The velocity profile is shown only up to the first velocity minimum (first part of the trajectories during backtracing). The color bar indicates the particle counts observed in a given energy and direction bin of SWIM that are backtraced.

energy flux over energy (> 1800 eV) and assuming an angular distribution of 30° × 30°, the flux of these suprathermal ions is ~ 1.2×10^5 cm^{-2} s^{-1}. With an average ion speed of 700 km s^{-1} (or energy of 2500 eV), the density of the ions is estimated to be ~1.7×10^{-3} cm^{-3}. Concerning trajectories that terminate on the dayside lunar surface, it was found that these particles are observed in a single angular pixel of SWIM. With an angular pixel size of 10° × 10°, the estimated flux is ~ 2×10^3 cm^{-2} s^{-1}. This is ~0.001% of the solar wind flux (~ 2×10^8 cm^{-2} s^{-1}), and at least 2 orders of magnitude lower than the reported flux of solar wind protons scattered from the lunar surface, which is ~0.1–1% of the solar wind flux [*Saito et al.*, 2008]. Moreover, this is 2 orders lower than the flux of the observed suprathermal H^+, whose trajectories terminate well above the dayside lunar surface. Thus, it is concluded that the flux of particles originating at the surface cannot explain the observation.

The observation of a similar population of suprathermal ions of $m/q = 1$ in orbit 2264 on 14 May 2009 (Event 2), orbit 2098 on 30 April 2009 (Event 3), and orbit 2040 on 25 April 2009 (Event 4) are presented in the supporting information (Figures S2–S7).

In order to understand the sensitivity of the backtracing results on the adopted values of B_{wake} and E_{wake}, we performed the simulations varying both parameters for all the events (Event 1 to Event 4). The values for B_{wake} include $1.0 \times B_{IMF}$, $1.5 \times B_{IMF}$, and $2.0 \times B_{IMF}$. For E_{wake}, we considered the values $0.5 \times E_{wakeref}$, $1.0 \times E_{wakeref}$, $1.5 \times E_{wakeref}$, and $2.0 \times E_{wakeref}$, where $E_{wakeref} = 0.7$ mV m^{-1} [*Halekas et al.*, 2005; *Nishino et al.*, 2009b; *Dhanya et al.*, 2016]. For the entire ranges of B_{wake} and E_{wake}, the major source of the observed ions is located at high altitude (>500 km) above the dayside lunar surface. The details are presented in the supporting information (section 4).

Considering the observations in several orbits, the observed flux of the suprathermal H^+ populations is in the range of $\sim 1.5 \times 10^4$ to 2.5×10^5 cm^{-2} s^{-1} ($\sim 10^{-4}$ to 10^{-5} of the solar wind flux) and translates into a density $\sim 2 \times 10^{-4}$ to 3.5×10^{-3} cm^{-3}.

4. Discussion

The adopted mass $m/q = 1$ is consistent with hydrogen ions. *Futaana et al.* [2010] have discussed the observation of accelerated protons around the Moon from SARA, and these were interpreted to be associated with surface-scattered solar wind protons [*Saito et al.*, 2008] that subsequently move under the forces of E_c and B_{IMF}. For the events reported here, the fraction of H^+ ions that terminate on the lunar surface at the end of backtracing is too low (<0.001% of the solar wind flux) to explain the observations. The source of the suprathermal H^+ ions, with initial velocities as high as the solar wind velocity originating at altitudes >500 km above the dayside lunar surface is not known and needs to be investigated.

The details of the lunar magnetic anomalies are not included in the backtracing model. However, considering the limited spatial extent of these anomalies, low field strength, and the decrease in magnitude as a function of altitude, the magnetic anomalies may significantly affect the particle trajectories only within 50 km from the surface. To account for this, we performed backtracing simulations after increasing the lunar radius by 50 km, but the results did not change significantly.

Upon interaction with the lunar regolith, the solar wind protons backscatter as energetic neutral hydrogen atoms (H_{ENA}) with a reflection ratio of 10–20% [*McComas et al.*, 2009; *Wieser et al.*, 2009; *Vorburger et al.*, 2013; *Bhardwaj et al.*, 2015]. These lunar H_{ENA} with energies almost 50% of that of solar wind travel to space without any perturbation. Since H_{ENA} can become ionized [*Funsten et al.*, 2013] and hence travel back to the Moon under B_{IMF} and E_c, they are considered as a possible source of the observed suprathermal H^+. The solar wind fluxes during the events are in the range $(2–3) \times 10^8$ cm^{-2} s^{-1}. The maximum flux of backscattered H_{ENA} would be $\sim(4–6) \times 10^7$ cm^{-2} s^{-1} (20% of the solar wind flux). The ionization includes photoionization, solar wind charge exchange, and solar wind electron impact ionization. We adopted the ionization rates reported for interplanetary H_{ENA} at 1 AU (that are associated with inner source pickup ions), with a photoionization rate of 0.62×10^{-7} s^{-1} for quiet Sun condition and electron impact ionization rate of 0.65×10^{-7} s^{-1} [*Bochsler and Möbius*, 2010; http://phidrates.space.swri.edu]. The solar wind charge exchange depends on the relative velocity of the H_{ENA} and solar wind protons. The average solar wind speeds during the observed events are in the range of 300–400 km s^{-1}. With an energy loss of 50%, the H_{ENA} can have an average speed of ~220–280 km s^{-1}. Using the cross-section values and the expression for the ionization rate given in *Bzowski* [2008], we estimated the solar wind charge exchange rate to be $\sim 4 \times 10^{-7}$ s^{-1} for the case when H_{ENA} and solar wind are traveling antiparallel (maximum relative velocity). We consider a $1/r^2$ fall off in the density of H_{ENA}, where r is the radial distance from the Moon center. Thus, at the altitude range 500–2000 km, the density of H_{ENA} is ~(0.75–0.25) times the density near the surface. The H^+_{ENA} flux is obtained as $J = \int n(z)\beta dz$, where n is the H_{ENA} density as a function of altitude (z), β the ionization rate, and dz the altitude element. Using the density and ionization rates introduced above, the resulting ion flux in the altitude range of 500–2000 km is ~100–150 cm^{-2} s^{-1}. This is too low compared to the observed flux of suprathermal H^+.

H^+ ions produced from the ionization of lunar exospheric H are considered next. With a surface density value of ~10–24 cm^{-3} for lunar exospheric hydrogen [*Cook et al.*, 2013; *Hartle and Thomas*, 1974; *Wurz et al.*, 2007], scale height of 1000 km, and ionization rate of 10^{-7} cm^{-3}, the flux of H^+ from the ionization of the lunar exosphere is estimated to be 1.4×10^2 cm^{-2} s^{-1}, which is much smaller compared to the observed flux. Moreover, the high initial velocities of the observed ions also do not favor an exospheric source.

Another possible source could be inner source pickup hydrogen ions (inner source PUI) that have been observed to exist within a distance of 4 AU from the Sun [*Geiss et al.*, 1995; *Gloeckler et al.*, 2000; *Schwadron et al.*, 2000; *Gruntman and Izmodenov*, 2004; *Bochsler and Möbius*, 2010]. Inner source PUIs can have initial velocities comparable to that of solar wind and may access the lunar environment due to their trajectories under B_{IMF} and E_c. The estimated density of inner source H^+ at 1 AU from the ionization of ENAs is $\sim 7 \times 10^{-4}$ cm^{-3} [*Schwadron and McComas*, 2010]. Compared with the observed densities of the suprathermal H^+, inner source PUIs appear to contribute to the events of lower density (similar to Event 3 and Event 4), whereas they cannot explain the events with higher density of suprathermal H^+ (similar to Events 1 and 2). However, the bulk of the inner source PUIs move with the solar wind and hence are likely to have an initial velocity parallel to solar wind as opposed to the observed ions which have initial velocity antiparallel to the solar wind. Thus, the velocity distribution of the observed ions does not support inner source PUIs as the source although the density may be comparable for some of the events.

Interstellar pickup H^+ generated from ionization of interstellar neutral hydrogen at 1 AU could also be a possible source. However, due to various ionization processes, the survival probability of interstellar H is low while traversing to a distance of 1 AU. With the reported neutral hydrogen flux of ~800 cm^{-2} s^{-1} at 1 AU based on Interstellar Boundary Explorer measurements [*Saul et al.*, 2013], even assuming complete ionization of this neutral hydrogen at 1 AU would produce a flux at least 2 orders of magnitude lower than the observed value.

Between the Sun and the orbit of Earth, a neutral solar wind component exists with a fraction of 10^{-5} to 10^{-3} of the solar wind [*Collier et al.*, 2001]. The H^+ flux generated by the ionization of neutral solar wind at 1 AU is $\sim 10^2$ to 10^4 cm^{-2} s^{-1}, which is smaller than the observed flux by 1 to 3 orders of magnitude. Moreover, the neutral solar wind is unlikely to explain the suprathermal H^+, as these require a source with initial velocities antiparallel to the solar wind.

Because the Moon was close to the Earth's bow shock for some of the events (Figures 1f, S2f, and S4b), the possibility of solar wind protons reflected from Earth's bow shock [*Asbridge et al.*, 1968; *Lin et al.*, 1974] is considered. Such protons in the lunar environment have been reported from the Apollo SIDE experiment on the lunar surface [*Benson et al.*, 1975]. Solar wind protons reflected from the Earth's bow shock are known to consist of two populations—reflected and diffused with ~1% of solar wind density [*Gosling et al.*, 1978; *Paschmann et al.*, 1981; *Bonifazi and Moreno*, 1981a, 1981b]. The reflected population is generally of lower energy (1–7 keV/q) with sharply peaked energy spectra, in the form of a narrow beam [*Sonnerup*, 1969]. The energy range, high v_β (as high as 400 km s^{-1}), and the narrow angular spread of the SWIM-observed H^+ seems to be consistent with that of a reflected ion population. However, the reflected population moves dominantly along B_{IMF}, and hence, in the solar wind rest frame such a population is expected to have dominant $v_{\|}$ and negligible $v_{\perp}$, which is not supported by the observed distribution for any of the events.

Thus, the observation of suprathermal H^+ calls for an additional source to fully explain the population.

It is to be noted that SWIM was operated such that the suprathermal H^+ with energy up to 3.3 keV could be observed. However, due to acceleration under E_c, such a population can have energies >3.3 keV, which could not be observed by SWIM. Hence, the suprathermal H^+ population may show up more frequently in the observations with an ion mass analyzer of wider energy range around the Moon.

5. Conclusion

Suprathermal ions with energies 1.5–3 times the solar wind energy have been observed by SWIM in several orbits of Chandrayaan-1, when the Moon was located outside Earth's bow shock. Analysis shows that the ions have a mass to charge ratio of unity ($m/q = 1$), and they travel under interplanetary magnetic field and convective electric field of solar wind forming a ring-shaped velocity distribution. The ions have a high initial velocity in the range >100 km s^{-1} extending to the solar wind velocity, and in a direction antiparallel to that of solar wind. Backtracing simulations show that the suprathermal H^+ ions originate at altitudes >500 km above the dayside lunar surface in the direction of the solar wind. Sources considered to explain these ions are ionization of backscattered hydrogen ENAs from the Moon, ionization of lunar exospheric hydrogen, inner source pickup ions, interstellar pickup ions, ionization of neutral solar wind, and the solar wind protons reflected from Earth's bow shock. We have compared the flux (density) expected from these sources with the observation. We suggest that an additional source is required to fully explain the suprathermal H^+ population.

Acknowledgments
We thank the ACE SWEPAM instrument team, ACE MAG instrument team, and the ACE Science Center for providing the ACE data (http://www.srl.caltech.edu/ACE/ASC/level2/lvl2DATA_MAG-SWEPAM.html). We thank the Wind team and MIT Space Plasma Group for the Wind data (ftp://space.mit.edu/pub/plasma/wind/kp_files/). Chandrayaan-1 data are available for public at Indian Space Science Data Center (ISSDC). The efforts at Space Physics Laboratory of Vikram Sarabhai Space Centre are supported by the Indian Space Research Organization (ISRO). The effort at the University of Bern was supported in part by ESA and by the Swiss National Science Foundation.

References

Asbridge, J. R., S. J. Bame, and I. B. Strong (1968), Outward flow of protons from the Earth's bow shock, *J. Geophys. Res.*, *73*, 5777–5782, doi:10.1029/JA073i017p05777.

Barabash, S., et al. (2009), Investigation of the solar wind-Moon interaction onboard Chandrayaan-1 mission with the SARA experiment, *Curr. Sci.*, *96*(4), 526–532.

Benson, J., J. W. Freeman, H. K. Hills, and R. R. Vondrak (1975), Bow shock protons in the lunar environment, *Moon*, *14*, 19–25, doi:10.1007/BF00562969.

Bhardwaj, A., S. Barabash, Y. Futaana, Y. Kazama, K. Asamura, D. McCann, R. Sridharan, M. Holmström, P. Wurz, and R. Lundin (2005), Low energy neutral atom imaging on the Moon with the SARA instrument aboard Chandrayaan-1 mission, *J. Earth Syst. Sci.*, *114*, 749–760, doi:10.1007/BF02715960.

Bhardwaj, A., et al. (2012), Interaction of solar wind with Moon: An overview on the results from the SARA experiment aboard Chandrayaan-1, *Adv. Geosci.*, *30*, 35–55, doi:10.1142/9789814405744_0004.

Bhardwaj, A., et al. (2015), A new view on solar wind interaction with Moon, *Geosci. Lett.*, *2*, 1–15, doi:10.1186/s40562-015-0027-y.

Bochsler, P., and E. Möbius (2010), Energetic neutral atoms: An additional source for heliospheric pickup ions, *Astrophys. J. Lett.*, *721*, L6–L9, doi:10.1088/2041-8205/721/1/L6.

Bonifazi, C., and G. Moreno (1981a), Reflected and diffuse ions backstreaming from the Earth's bow shock: 1. Basic properties, *J. Geophys. Res.*, *86*, 4397–4413, doi:10.1029/JA086iA06p04397.

Bonifazi, C., and G. Moreno (1981b), Reflected and diffuse ions backstreaming from the Earth's bow shock: 2. Origin, *J. Geophys. Res.*, *86*, 4405–4414, doi:10.1029/JA086iA06p04405.

Bzowski, M. (2008), Survival probability and energy modification of hydrogen energetic neutral atoms on their way from the termination shock to Earth orbit, *Astron. Astrophys.*, *488*, 1057–1068, doi:10.1051/0004-6361:200809393.

Colburn, D. S., R. G. Currie, J. D. Mihalov, and C. P. Sonett (1967), Diamagnetic solar wind cavity discovered behind the Moon, *Science*, *158*, 1040–1042, doi:10.1126/science.158.3804.1040.

Collier, M. R., et al. (2001), Observations of neutral atoms from the solar wind, *J. Geophys. Res.*, *106*, 24,893–24,906, doi:10.1029/2000JA000382.

Cook, J. C., S. A. Stern, P. D. Feldman, G. R. Gladstone, K. D. Retherford, and C. C. C. Tsang (2013), New upper limits on numerous atmospheric species in the native lunar atmosphere, *Icarus*, *225*, 681–687, doi:10.1016/j.icarus.2013.04.010.

Dhanya, M. B., A. Bhardwaj, Y. Futaana, S. Fatemi, M. Holmström, S. Barabash, M. Wieser, P. Wurz, A. Alok, and R. S. Thampi (2013), Proton entry into the near-lunar plasma wake for magnetic field aligned flow, *Geophys. Res. Lett.*, *40*, 2913–2917, doi:10.1002/grl.50617.

Dhanya, M. B., A. Bhardwaj, Y. Futaana, S. Barabash, A. Alok, M. Wieser, M. Holmström, and P. Wurz (2016), Characteristics of proton velocity distribution functions in the near-lunar wake from Chandrayaan-1/SWIM observations, *Icarus*, *271*, 120–130, doi:10.1016/j.icarus.2016.01.032.

Funsten, H. O., et al. (2013), Reflection of solar wind hydrogen from the lunar surface, *J. Geophys. Res. Planets*, *118*, 292–305, doi:10.1002/jgre.20055.

Futaana, Y., S. Machida, Y. Saito, A. Matsuoka, and H. Hayakawa (2003), Moon-related nonthermal ions observed by Nozomi: Species, sources, and generation mechanisms, *J. Geophys. Res.*, *108*, 1025, doi:10.1029/2002JA009366.

Futaana, Y., S. Barabash, M. Wieser, M. Holmström, A. Bhardwaj, M. B. Dhanya, R. Sridharan, P. Wurz, A. Schaufelberger, and K. Asamura (2010), Protons in the near-lunar wake observed by the Sub-keV Atom Reflection Analyzer on board Chandrayaan-1, *J. Geophys. Res.*, *115*, A10248, doi:10.1029/2010JA015264.

Geiss, J., G. Gloeckler, L. A. Fisk, and R. von Steiger (1995), C^+ pickup ions in the heliosphere and their origin, *J. Geophys. Res.*, *100*, 23,373–23,378, doi:10.1029/95JA03051.

Gloeckler, G., L. A. Fisk, J. Geiss, N. A. Schwadron, and T. H. Zurbuchen (2000), Elemental composition of the inner source pickup ions, *J. Geophys. Res.*, *105*, 7459–7464, doi:10.1029/1999JA000224.

Gosling, J. T., J. R. Asbridge, S. J. Bame, G. Paschmann, and N. Sckopke (1978), Observations of two distinct populations of bow shock ions in the upstream solar wind, *Geophys. Res. Lett.*, *5*, 957–960, doi:10.1029/GL005i011p00957.

Gruntman, M., and V. Izmodenov (2004), Mass transport in the heliosphere by energetic neutral atoms, *J. Geophys. Res.*, *109*, A12108, doi:10.1029/2004JA010727.

Halekas, J. S., S. D. Bale, D. L. Mitchell, and R. P. Lin (2005), Electrons and magnetic fields in the lunar plasma wake, *J. Geophys. Res.*, *110*, A07222, doi:10.1029/2004JA010991.

Halekas, J. S., Y. Saito, G. T. Delory, and W. M. Farrell (2011), New views of the lunar plasma environment, *Planet. Space Sci.*, *59*, 1681–1694, doi:10.1016/j.pss.2010.08.011.

Halekas, J. S., A. R. Poppe, G. T. Delory, M. Sarantos, and J. P. McFadden (2013), Using ARTEMIS pickup ion observations to place constraints on the lunar atmosphere, *J. Geophys. Res. Planets*, *118*, 81–88, doi:10.1029/2012JE004292.

Halekas, J. S., M. Benna, P. R. Mahaffy, R. C. Elphic, A. R. Poppe, and G. T. Delory (2015), Detections of lunar exospheric ions by the LADEE neutral mass spectrometer, *Geophys. Res. Lett.*, *42*, 5162–5169, doi:10.1002/2015GL064746.

Halekas, J. S., A. R. Poppe, W. M. Farrell, and J. P. McFadden (2016), Structure and composition of the distant lunar exosphere: Constraints from ARTEMIS observations of ion acceleration in time-varying fields, *J. Geophys. Res. Planets*, *121*, 1102–1115, doi:10.1002/2016JE005082.

Hartle, R. E., and G. E. Thomas (1974), Neutral and ion exosphere models for lunar hydrogen and helium, *J. Geophys. Res.*, *79*, 1519–1526, doi:10.1029/JA079i010p01519.

Hilchenbach, M., D. Hovestadt, B. Klecker, and E. Moebius (1992), Detection of singly ionized energetic lunar pick-up ions upstream of Earth's bow shock, in *Solar Wind Seven Colloquium*, edited by E. Marsch and R. Schwenn, pp. 349–355, Pergamon Press, Goslar, Germany.

Holmström, M., M. Wieser, S. Barabash, Y. Futaana, and A. Bhardwaj (2010), Dynamics of solar wind protons reflected by the Moon, *J. Geophys. Res.*, *115*, A06206, doi:10.1029/2009JA014843.

Lin, R. P., C.-I. Meng, and K. A. Anderson (1974), 30- to 100-keV protons upstream from the Earth's bow shock, *J. Geophys. Res.*, *79*, 489–498, doi:10.1029/JA079i004p00489.

Lue, C., Y. Futaana, S. Barabash, M. Wieser, M. Holmström, A. Bhardwaj, M. B. Dhanya, and P. Wurz (2011), Strong influence of lunar crustal fields on the solar wind flow, *Geophys. Res. Lett.*, *38*, L03202, doi:10.1029/2010GL046215.

Mall, U., E. Kirsch, K. Cierpka, B. Wilken, A. Söding, F. Neubauer, G. Gloeckler, and A. Galvin (1998), Direct observation of lunar pick-up ions near the Moon, *Geophys. Res. Lett.*, *25*, 3799–3802, doi:10.1029/1998GL900003.

McComas, D. J., et al. (2009), Global observations of the interstellar interaction from the Interstellar Boundary Explorer (IBEX), *Science*, *326*, 959–962, doi:10.1126/science.1180906.

Nishino, M. N., et al. (2009a), Pairwise energy gain-loss feature of solar wind protons in the near-Moon wake, *Geophys. Res. Lett.*, *36*, L12108, doi:10.1029/2009GL039049.
Nishino, M. N., et al. (2009b), Solar-wind proton access deep into the near-Moon wake, *Geophys. Res. Lett.*, *36*, L16103, doi:10.1029/2009GL039444.
Paschmann, G., N. Sckopke, I. Papamastorakis, J. R. Asbridge, S. J. Bame, and J. T. Gosling (1981), Characteristics of reflected and diffuse ions upstream from the Earth's bow shock, *J. Geophys. Res.*, *86*, 4355–4364, doi:10.1029/JA086iA06p04355.
Poppe, A. R., J. S. Halekas, J. R. Szalay, M. Horányi, Z. Levin, and S. Kempf (2016), LADEE/LDEX observations of lunar pickup ion distribution and variability, *Geophys. Res. Lett.*, *43*, 3069–3077, doi:10.1002/2016GL068393.
Richmond, N. C., and L. L. Hood (2008), A preliminary global map of the vector lunar crustal magnetic field based on Lunar Prospector magnetometer data, *J. Geophys. Res.*, *113*, E02010, doi:10.1029/2007JE002933.
Saito, Y., et al. (2008), Solar wind proton reflection at the lunar surface: Low energy ion measurement by MAP-PACE onboard SELENE (KAGUYA), *Geophys. Res. Lett.*, *35*, L24205, doi:10.1029/2008GL036077.
Saito, Y., et al. (2010), In-flight performance and initial results of Plasma energy angle and composition experiment (PACE) on SELENE (Kaguya), *Space Sci. Rev.*, *154*, 265–303, doi:10.1007/s11214-010-9647-x.
Saul, L., M. Bzowski, S. Fuselier, M. Kubiak, D. McComas, E. Möbius, J. Sokół, D. Rodríguez, J. Scheer, and P. Wurz (2013), Local interstellar hydrogen's disappearance at 1 AU: Four years of IBEX in the rising solar cycle, *Astrophys. J.*, *767*, 130, doi:10.1088/0004-637X/767/2/130.
Schwadron, N. A., and D. J. McComas (2010), Pickup ions from energetic neutral atoms, *Astrophys. J. Lett.*, *712*, L157–L159, doi:10.1088/2041-8205/712/2/L157.
Schwadron, N. A., J. Geiss, L. A. Fisk, G. Gloeckler, T. H. Zurbuchen, and R. von Steiger (2000), Inner source distributions: Theoretical interpretation, implications, and evidence for inner source protons, *J. Geophys. Res.*, *105*, 7465–7472, doi:10.1029/1999JA000225.
Sonnerup, B. U. Ö. (1969), Acceleration of particles reflected at a shock front, *J. Geophys. Res.*, *74*, 1301–1304, doi:10.1029/JA074i005p01301.
Stern, S. A. (1999), The lunar atmosphere: History, status, current problems, and context, *Rev. Geophys.*, *37*, 453–492, doi:10.1029/1999RG900005.
Tsunakawa, H., F. Takahashi, H. Shimizu, H. Shibuya, and M. Matsushima (2015), Surface vector mapping of magnetic anomalies over the Moon using Kaguya and Lunar Prospector observations, *J. Geophys. Res. Planets*, *120*, 1160–1185, doi:10.1002/2014JE004785.
Vorburger, A., P. Wurz, S. Barabash, M. Wieser, Y. Futaana, C. Lue, M. Holmström, A. Bhardwaj, M. B. Dhanya, and K. Asamura (2013), Energetic neutral atom imaging of the lunar surface, *J. Geophys. Res. Space Physics*, *118*, 3937–3945, doi:10.1002/jgra.50337.
Wang, X.-D., et al. (2010), Acceleration of scattered solar wind protons at the polar terminator of the Moon: Results from Chang'E-1/SWIDs, *Geophys. Res. Lett.*, *37*, L07203, doi:10.1029/2010GL042891.
Wang, X.-D., et al. (2011), Detection of $m/q = 2$ pickup ions in the plasma environment of the Moon: The trace of exospheric H_2^+, *Geophys. Res. Lett.*, *38*, L14204, doi:10.1029/2011GL047488.
Wieser, M., and S. Barabash (2016), A family for miniature, easily reconfigurable particle sensors for space plasma measurements, *J. Geophys. Res. Space Physics*, *121*, 11,588–11,604, doi:10.1002/2016JA022799.
Wieser, M., S. Barabash, Y. Futaana, M. Holmström, A. Bhardwaj, R. Sridharan, M. B. Dhanya, P. Wurz, A. Schaufelberger, and K. Asamura (2009), Extremely high reflection of solar wind protons as neutral hydrogen atoms from regolith in space, *Planet. Space Sci.*, *57*, 2132–2134, doi:10.1016/j.pss.2009.09.012.
Wurz, P., U. Rohner, J. A. Whitby, C. Kolb, H. Lammer, P. Dobnikar, and J. A. Martín-Fernández (2007), The lunar exosphere: The sputtering contribution, *Icarus*, *191*, 486–496, doi:10.1016/j.icarus.2007.04.034.